Vortex patterns and the critical rotational frequency in rotating dipolar Bose-Einstein condensates

Yongyong Cai, Yongjun Yuan, Matthias Rosenkranz, Han Pu, and Weizhu Bao

Phys. Rev. A **98**, 023610 — Published 10 August 2018

DOI: 10.1103/PhysRevA.98.023610

Vortex patterns and the critical rotational frequency in rotating dipolar Bose-Einstein condensates

Yongyong Cai,[1] Yongjun Yuan,[2,*] Matthias Rosenkranz,[3] Han Pu,[4] and Weizhu Bao[3]

[1]*Beijing Computational Science Research Center, Haidian District, Beijing 100193, People's Republic of China*
[2]*Key Laboratory of High Performance Computing and Stochastic Information Processing (Ministry of Education of China), College of Mathematics and Statistics, Hunan Normal University, Changsha, Hunan 410081, People's Republic of China*
[3]*Department of Mathematics, National University of Singapore, 119076, Singapore*
[4]*Department of Physics and Astronomy, and Rice Quantum Institute, Rice University, Houston, TX 77251, USA*

(Dated: July 23, 2018)

Based on the two-dimensional mean-field equations for pancake-shaped dipolar Bose-Einstein condensates in a rotating frame, for both attractive and repulsive dipole-dipole interaction (DDI) as well as arbitrary polarization direction, we study the profiles of the single vortex state and show how the critical rotational frequency change with the s-wave contact interaction strength, DDI strength and the polarization angle. In addition, we find numerically that at the 'magic angle' $\vartheta = \arccos(\sqrt{3}/3)$, the critical rotational frequency is almost independent of the DDI strength. By numerically solving the dipolar Gross-Pitaevskii Equation at high rotation speed, we identify different patterns of vortex lattices which strongly depend on the polarization direction. As a result, we undergo a study of vortex lattice structures for the whole regime of polarization direction and find evidence that the vortex lattice orientation tends to be aligned to the dipole polarization axis for positive DDI strength and to the perpendicular direction of the dipole axis for negative DDI strength.

PACS numbers: 03.75.Hh, 75.80.+q, 67.85.-d

I. INTRODUCTION

One of the striking features of rotating atomic Bose-Einstein condensates (BECs) is the formation of vortices above a critical angular velocity [1–3]. In a symmetric BEC, multiple vortices arrange in a characteristic triangular pattern [2]. This triangular vortex lattice minimizes the free energy of the BEC.

While the initial experiments considered atoms with local interactions, more recently, dipolar BECs with significant electric or magnetic dipole moment have received much attention from both theoretical and experimental studies (for recent reviews, see Refs. [4, 5]). The dipole-dipole interaction (DDI) crucially affects the ground-state properties [6, 7], stability [8–11], and dynamics of the gas [12]. Furthermore, they offer a route for studying many-body quantum effects, such as a superfluid-to-crystal quantum phase transition [13], supersolids [14] or even topological quantum phases [15]. Recent advances in experimental techniques have paved the way for a Bose-Einstein condensate (BEC) of ^{52}Cr with a magnetic dipole moment $6\mu_B$ (Bohr magneton μ_B), much larger than conventional alkali BECs [16–18]. Promising candidates for dipolar BEC experiments are Er and Dy with even larger magnetic moments of $7\mu_B$ and $10\mu_B$, respectively, which have been reported in experiments [19, 20]. Furthermore, DDI-induced decoherence and spin textures have been observed in alkali-metal condensates [21, 22]. Dipolar effects also play a crucial role in experiments with Rydberg atoms [23] and heteronuclear molecules [24, 25]. Bosonic heteronuclear molecules may provide a basis for future experiments on BECs with dipole moments much larger than those in atomic BECs [26].

The anisotropy of DDI dramatically affects stationary states of the rotating dipolar BEC. In this article we focus on a system of dipolar BEC confined in a quasi-two-dimensional pancake shaped trapping potential with the atomic magnetic dipoles polarized by an external magnetic field. We define the polarization angle ϑ to be the angle between the dipoles and the normal direction of the condensate plane. Hence, if the dipoles lie in the plane of the condensate, we have $\vartheta = \pi/2$; whereas if the dipoles are perpendicular to the plane, we have $\vartheta = 0$. By adjusting the external magnetic field, ϑ can be varied smoothly between 0 and $\pi/2$. Most previous studies of rotating dipolar BECs focused only on the limiting cases with $\vartheta = 0$ or $\pi/2$ [27–31]. Recently, Zhao and Gu [32] and Malet *et al.* [33] studied the angular momentum and critical rotational frequency of a 2D dipolar BEC with positive DDI strength in the intermediate regime. Their results show that the critical rotational frequency monotonically increases with the polarization angle ϑ, while the relation between the critical rotational velocity and the DDI strength is ϑ-dependent. Martin *et al.* [34] analytically studied the vortex lattice for the case where the dipoles are not perpendicular to the plane of rotation, and suggested that there is a phase transition in the lattice geometry from triangle to square which can be measured as a function of the DDI strength, and the vortex lattice orientation does not depend on the polarization angle ϑ. This vortex structure transition was observed in the numerical results of Zhao and Gu [32] for a rotating quasi-2D dipolar BEC with positive DDI strength, however, to our knowledge, there have not, to date, been numerical results concerning the change of vortex lattice orientation with respect to the polarization angle ϑ. In this paper, we further study the impacts of the s-wave contact interaction strength and the polarization angle on the critical rotational frequency for both positive and negative DDI, and focus on vortex lattice structure with many vortices in the fast rotation limit. Different patterns of vortex lattices are ob-

* Corresponding Author (yuanyongjun0301@163.com)

served, which strongly depend on the polarization direction and we characterize the vortex lattice structure by virtue of the static structure factor [35, 36]. We also take into account negative DDI which can be achieved with a rotating magnetic field [37]. Simulating high vortex numbers requires reliable numerical methods. We employed spectral methods that are very accurate for such kinds of problems [38–42], with less grid points needed than those of traditional finite difference methods.

This article is organized as follows. In Sec. II we present a 2D model for a dipolar BEC in the rotating frame. We also explain our approach for numerically solving this model. In Sec. III, we show how the s-wave contact interaction strength and the polarization angle affect the critical rotational frequency with both attractive and repulsive DDI strengths. In Sec. IV we present simulation results of stationary states at high rotation frequency for different polarization angles and DDI strengths. Focusing on the regime with many vortices allows us to discern characteristic vortex patterns that occur as the polarization changes from predominantly perpendicular to parallel. We conclude in Sec. V.

II. MODEL

We consider a polarized dipolar BEC trapped in a cylindrically symmetric harmonic potential $\tilde{V}(\boldsymbol{r}) = \frac{1}{2}m[\omega_r^2(x^2+y^2)+\omega_z^2 z^2]$ with m the atomic mass and ω_r, ω_z the transverse and axial trap frequencies, respectively. We assume that the magnetic dipoles are polarized along an axis $\mathbf{n} = (\cos\varphi\sin\vartheta, \sin\varphi\sin\vartheta, \cos\vartheta)$, where φ and ϑ are the azimuthal and polar angles, respectively. The DDI potential between two atoms separated by the relative vector $\boldsymbol{r}$ is given by

$$U_{\rm dd}(\boldsymbol{r}) = \frac{g_d}{4\pi}\frac{1-3\cos^2\theta}{|\boldsymbol{r}|^3}. \tag{1}$$

Here, θ is the angle between the polarization axis $\mathbf{n}$ and $\boldsymbol{r}$. For magnetic dipoles, the interaction strength g_d is given by $g_d = \mu_0\mu_d^2$, where μ_0 is the magnetic vacuum permeability and μ_d is the dipole moment. In addition, we assume that the BEC is rotating with frequency Ω around the z axis. In the remainder of this article we adopt length, time and energy units as $a_r = \sqrt{\hbar/m\omega_r}$, $1/\omega_r$, and $\hbar\omega_r$, respectively. At zero temperature this dipolar BEC system is described by the Gross-Pitaevskii equation (GPE) in the rotating frame [12, 43]

$$\begin{aligned} i\partial_t\Psi(\boldsymbol{r},t) = \Big[-\frac{1}{2}\nabla^2 + V(\boldsymbol{r}) - \Omega L_z + g|\Psi|^2 \\ + \int d\boldsymbol{r}' U_{\rm dd}(\boldsymbol{r}-\boldsymbol{r}')|\Psi(\boldsymbol{r}',t)|^2\Big]\Psi(\boldsymbol{r},t). \end{aligned} \tag{2}$$

Here, $L_z = i(y\partial_x - x\partial_y)$ is the z component of the angular momentum operator and $g = 4\pi N a_s/a_r$ with N being the number of atoms and a_s being the s-wave scattering length. The dimensionless DDI strength is given by $g_d = Nm\mu_0\mu_d^2/3\hbar^2 a_r$, and the potential is $V(\boldsymbol{r}) = \frac{1}{2}(x^2+y^2) + \frac{\omega_z^2}{2\omega_r^2}z^2$. It is noted that both the sign and the magnitude of the DDI strength g_d could be modified through a rotating magnetic field [37]. In addition, a dipolar BEC system described by Eq.(2) is stable, i.e. admits ground states, if and only if $\varepsilon_{\rm dd} = \frac{g_{\rm dd}}{g} \in [-\frac{1}{2}, 1]$ [39] and $|\Omega| < 1$. Therefore, we will focus on the typical parameters within this range[44].

We consider the quasi-2D regime where $\omega_z \gg \omega_r$, and the interactions are sufficiently weak such that no axial modes are excited [45]. In this regime, the wave function $\Psi(\boldsymbol{r},t)$ can be separated into a transverse and a longitudinal part, that is, $\Psi(\boldsymbol{r},t) = \psi(\boldsymbol{\rho},t)w(z)\exp(-i\gamma t/2)$, where $\boldsymbol{\rho} = (x,y)$, $|\boldsymbol{\rho}| = \sqrt{x^2+y^2}$, $w(z) = (\gamma/\pi)^{1/4}\exp(-z^2/2\gamma)$ is the ground mode in z direction, and $\gamma = \omega_z/\omega_r$. Inserting this expansion of the wave function into Eq. (2) and integrating out the z variable reduces Eq. (2) to [46, 47]

$$\begin{aligned} i\partial_t\psi(\boldsymbol{\rho},t) = \Big[-\frac{1}{2}\nabla_r^2 + \frac{|\boldsymbol{\rho}|^2}{2} - \Omega L_z + \bar{g}|\psi(\boldsymbol{\rho},t)|^2 \\ + \int d\boldsymbol{\rho}' U_{\rm dd}^{\rm 2D}(\boldsymbol{\rho}-\boldsymbol{\rho}')|\psi(\boldsymbol{\rho}',t)|^2\Big]\psi(\boldsymbol{\rho},t). \end{aligned} \tag{3}$$

Here, $\nabla_r^2 = \partial_x^2 + \partial_y^2$ and $\bar{g} = \sqrt{\frac{\gamma}{2\pi}}\left[g - g_d\left(1-3\cos^2\vartheta\right)\right]$ is the effective 2D contact interaction strength that now depends on the DDI strength and polarization direction. The effective kernel for the 2D DDI is given by

$$\begin{aligned} U_{\rm dd}^{\rm 2D}(\boldsymbol{\rho}) = \frac{g_d\gamma^{3/2}}{8\sqrt{2\pi^3}}e^{\gamma|\boldsymbol{\rho}|^2/4}\Big[\left(1-3\cos^2\vartheta+\gamma[(x\cos\varphi+y\sin\varphi)^2\sin^2\vartheta - |\boldsymbol{\rho}|^2\cos^2\vartheta]\right)K_0(\gamma|\boldsymbol{\rho}|^2/4) \\ -\left(1-\cos^2\vartheta+\gamma[(x\cos\varphi+y\sin\varphi)^2[1-2/\gamma|\boldsymbol{\rho}|^2]\sin^2\vartheta - |\boldsymbol{\rho}|^2\cos^2\vartheta]\right)K_1(\gamma|\boldsymbol{\rho}|^2/4)\Big], \end{aligned} \tag{4}$$

where K_ν are modified Bessel functions of the second kind. In Fourier space, the DDI potential $\int d\boldsymbol{\rho}' U_{\rm dd}^{\rm 2D}(\boldsymbol{\rho}-\boldsymbol{\rho}')|\psi(\boldsymbol{\rho}')|^2$ becomes $\hat{V}_{\rm 2D}(\boldsymbol{k}) = \hat{U}_{\rm dd}^{\rm 2D}(\boldsymbol{k})\widehat{|\psi|^2}(\boldsymbol{k})$ with $\widehat{|\psi|^2}(\boldsymbol{k})$ being the condensate density function in momentum space and $\hat{U}_{\rm dd}^{\rm 2D}(\boldsymbol{k}) = \frac{3g_d}{2}[(\hat{k}_x\cos\varphi + \hat{k}_y\sin\varphi)^2\sin^2\vartheta - \cos^2\vartheta]k e^{k^2/2\gamma}\,\mathrm{erfc}(k/\sqrt{2\gamma})$, where $k = |\boldsymbol{k}|$, $\hat{k}_{x,y} = k_{x,y}/k$ are normalized components of the momentum, and $\mathrm{erfc}(x) = 1-\mathrm{erf}(x)$ is the complementary error function.

For positive DDI $g_d > 0$, the effective nonlocal interaction of a quasi-2D dipolar BEC described by Eq. (4), is attractive along the projection of the polarization axis $(\cos\varphi, \sin\varphi)$ and

repulsive perpendicular to the polarization axis. For axial polarization $\vartheta = 0$, the nonlocal interaction is isotropic and repulsive. In our work, without loss of generality, we assume that the dipoles are polarized in the xz-plane, such that we can fix $\varphi = 0$, i.e. the dipole axis is $\mathbf{n} = (\sin\vartheta, 0, \cos\vartheta)$. The effective interaction diverges less strongly in the limit $|\boldsymbol{\rho}| \to 0$ than the full 3D dipole-dipole potential $U_{\rm dd}$. Furthermore, it has a well-behaved Fourier transform, which is advantageous for numerical computations [46]. To find the ground states, we use the imaginary time method [38–40], with backward Euler discretization in time and Fourier spectral discretization in space.

III. CRITICAL ROTATION FREQUENCY

In this section, we show the impacts of varying s-wave contact interaction strength g, DDI strength g_d and polarization angle ϑ on the critical rotational frequency, respectively. Malet *et al.* [33] have studied the angular momentum and critical rotational frequency of a dipolar BEC in the intermediate regime with positive DDI strength, here we further study it for rotating dipolar BECs with both positive and negative DDI. We are also interested in the change of the structure of a single vortex with different polarization angle ϑ.

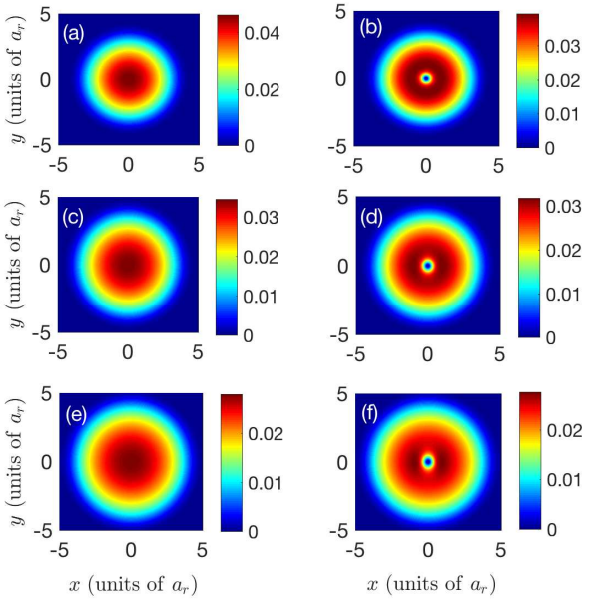

FIG. 1. (Color online) Density of a rotating dipolar BEC around the critical rotational frequency Ω_c for fixed $\gamma = 10$, $g = 250$, $g_d = -100$, different polarization axis $\mathbf{n} = (\sin\vartheta, 0, \cos\vartheta)$ ($\vartheta = 0$ top panel (a),(b); $\vartheta = \pi/4$ middle panel (c), (d); $\vartheta = \pi/2$ bottom panel, (e),(f)). The critical rotational frequency Ω_c is found to be $0.356 < \Omega_c < 0.357$ (top panel), $0.275 < \Omega_c < 0.276$ (middle panel), $0.236 < \Omega_c < 0.237$ (bottom panel), with the corresponding lower bound of rotational frequency for the non-vortex states and the upper bound for the vortex state.

Firstly, we study the density profiles of the condensate near the critical rotational frequency. It is observed that for the fixed effective 2D contact interaction strength $\bar{g}$ and the DDI strength g_d, there exists a critical rotation frequency Ω_c such that there is no vortex if $\Omega < \Omega_c$ and at least one vortex if $\Omega \geq \Omega_c$ [cf. e.g., Figs. 1(a)–(b) and 2(e)–(f)]. By varying the polarization angle ϑ from 0 (z direction out-of-plane polarization) to $\pi/2$ (x direction in-plane polarization), we examine the relation between the dipole polarization axis and the critical rotational frequency, and check how the anisotropic DDI changes the density profile of the single vortex state. Figures 1-2 display density plots of the rotating dipolar BEC near the critical rotational frequency with representative negative and positive DDI strength g_d, respectively.

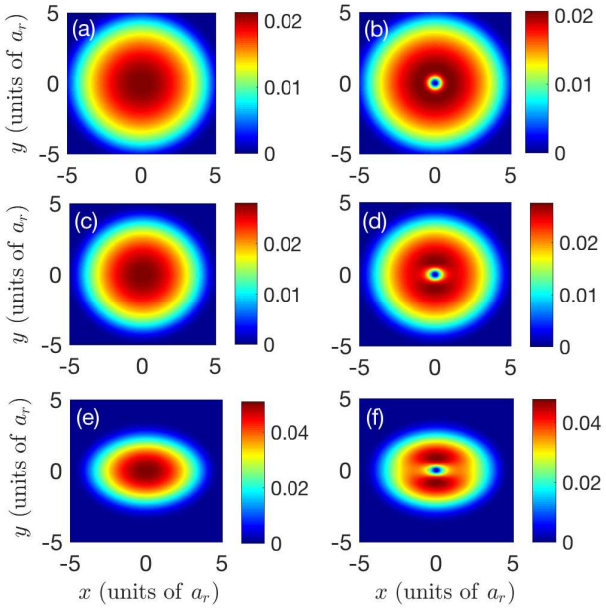

FIG. 2. (Color online) Density of a rotating dipolar BEC around the critical rotation frequency Ω_c for fixed $\gamma = 10$, $g = 250$, $g_d = 200$, different polarization axis $\mathbf{n} = (\sin\vartheta, 0, \cos\vartheta)$ ($\vartheta = 0$ top panel (a),(b); $\vartheta = \pi/4$ middle panel (c), (d); $\vartheta = \pi/2$ bottom panel, (e),(f)). The critical rotational frequency Ω_c is found to be $0.195 < \Omega_c < 0.196$ (top panel), $0.232 < \Omega_c < 0.233$ (middle panel), $0.357 < \Omega_c < 0.358$ (bottom panel), with the corresponding lower bound of rotational frequency for the non-vortex states and the upper bound for the vortex state.

At $\vartheta = 0$ when the dipoles are polarized perpendicular to the xy plane, Figs. 1-2 show that the 2D BEC is radially symmetric. This is expected as the 2D effective DDI and contact interaction are isotropic in this situation. Due to the anisotropy of the DDI, the profiles of the vortices change and become more anisotropic when the dipole axis tilts into the 2D BEC plane for increasing polarization angle ϑ. For negative (positive) DDI strength g_d, the Fourier transform of $U_{\rm dd}^{\rm 2D}$ (Eq. (4)) shows that the DDI induces a growing attractive (repulsive) interaction in x direction in terms of the energy contribution, for increasing $\vartheta : 0 \to \pi/2$. As a consequence, BEC becomes more compressed (elongated) in the x direction for negative (positive) g_d compared to the y direction. This is

in accordance with the fact that positive DDI tends to align the dipoles along the polarization axis in a head-to-tail manner ($\theta = 0, \pi$ in (1), preferable along x axis) and negative DDI tends to align the dipoles perpendicular to the polarization axis ($\theta = \pm\pi/2$ in (1), preferable along y axis). Moreover, the effective contact interaction $\bar{g}$ in Eq. (3) increases (decreases) for negative (positive) g_d with varying $\vartheta : 0 \to \pi/2$, which leads to the size change of BEC in Figs. 1-2.

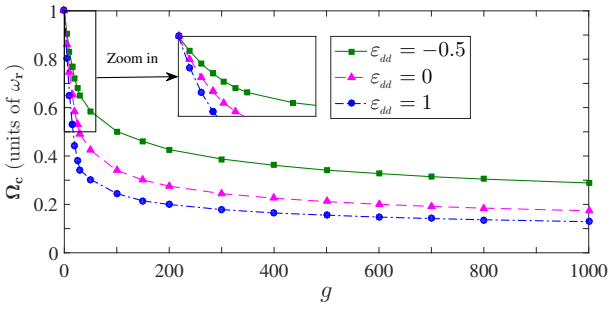

FIG. 3. The critical rotational frequency Ω_c of a rotating dipolar BEC v.s. the s-wave contact interaction strength $g = 4\pi N a_s/a_r$ for fixed $\gamma = 10$, dipole axis $\mathbf{n} = (0, 0, 1)$ and a natural dimensionless parameter $\varepsilon_{dd} := g_d/g =$ - 0.5, 0 and 1, respectively.

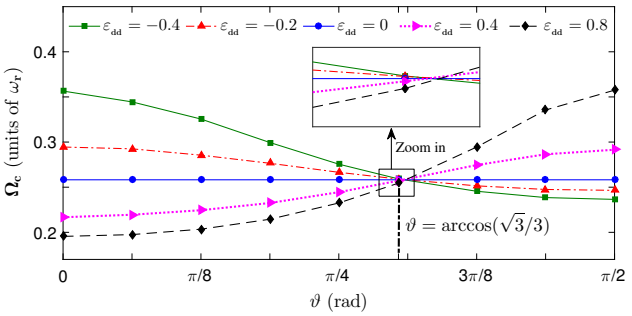

FIG. 4. The critical rotational frequency Ω_c of a rotating dipolar BEC v.s. polarization angle ϑ for fixed $\gamma = 10$, $g = 250$ and ε_{dd}= - 0.4, - 0.2, 0, 0.4 and 0.8, respectively.

Secondly, we investigate how the critical frequency Ω_c changes with interaction parameters g and g_d. For radially symmetric case with the dipoles polarized along the z axis (i.e., $\vartheta = 0$) and the varying contact interaction strength g with fixed $\varepsilon_{dd} = g_d/g$, where the DDI is isotropic in the xy plane, Figure 3 illustrates the dependence of the critical rotation frequency Ω_c on the s-wave contact interaction strength g. The numerical results show that Ω_c decreases when g increases for any fixed positive and negative DDI strength g_d. Furthermore, $\Omega_c \to 1$ as $g \to 0$ and Ω_c drops dramatically when g increases near $g \approx 0$. This is in accordance with the isotropic conventional rotating condensates without DDI [1–3]. It is also clear that when the DDI strength $g_d \nearrow$, $\Omega_c \searrow$ for any fixed s-wave contact interaction strength g and other parameters.

When tuning the dipole orientation $\mathbf{n} = (\sin\vartheta, 0, \cos\vartheta)$ by increasing the polarization angle ϑ from 0 to $\pi/2$, DDI induces an increasingly anisotropic interaction in xy plane and hence influences the critical rotational frequency Ω_c. Figure 4 shows Ω_c versus ϑ. It is observed that Ω_c decreases (increases) when effective contact interaction strength $\bar{g}$ increases (decreaes) with ϑ varying from 0 to $\pi/2$ for any fixed negative (positive) DDI strength g_d. Moreover, the curves of Ω_c as functions of ϑ with both negative and positive DDI strength g_d almost intersect with each other at the 'magic angle' $\vartheta = \arccos(\sqrt{3}/3)$. This can be understood as follows. At this angle the effective 2D contact interaction in Eq. (3) is independent of the DDI strength g_d, while the long range interaction part (the convolution term) in Eq. (3) is much weaker compared to the effective contact interaction part (cubic term), and thus has very little impact on the critical rotational frequency.

IV. VORTEX LATTICE PATTERNS UNDER FAST ROTATION

In this section, we show different vortex lattices that emerge as stationary states for varying polarization angles under fast rotation. To characterize the structure of the vortex lattice, we define the static structure factor [35, 36]

$$S(\boldsymbol{k}) = \frac{1}{N_v^2}\left|\sum_j e^{i\boldsymbol{k}\cdot\boldsymbol{\rho}_j}\right|^2, \tag{5}$$

where N_v is the number of vortices and $\boldsymbol{\rho}_j$ are the vortex core positions. The structure factor exhibits peaks at the reciprocal lattice sites, which reveal the frequencies and orientation of the vortex lattice. The reciprocal lattice is defined by two basis vectors $\boldsymbol{k}_1$ and $\boldsymbol{k}_2$. Here we choose $\boldsymbol{k}_1$ as the one closest to the y-axis and use the parameter $\eta = \angle(\boldsymbol{k}_1, \boldsymbol{k}_2)$ to characterize the orientation of the vortex lattice [c.f. Fig. 5]. $\eta = \pi/2$ for a rectangular vortex lattice, and $\pi/3$ for a trianglar lattice.

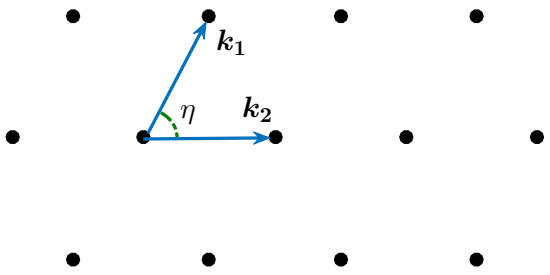

FIG. 5. Illustration of the Bravais lattice basis vectors and the lattice parameters.

We start with the impact of the polarization direction on the vortex lattice geometry. We compute the ground states of the dipolar BEC for different polarization angles ϑ at strong

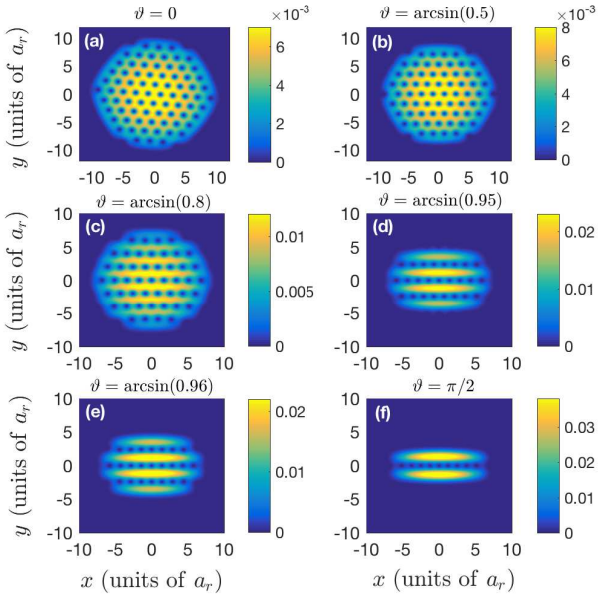

FIG. 6. (Color online) Density of a rotating dipolar BEC for different dipole polarization direction $\mathbf{n} = (\sin\vartheta, \mathbf{0}, \cos\vartheta)$, with $\vartheta = 0, \arcsin(0.5), \arcsin(0.8), \arcsin(0.95), \arcsin(0.96), \pi/2$. The rotational frequency is $\Omega = 0.95$, $\gamma = 10$, $g = 250$, and $g_d = 250$.

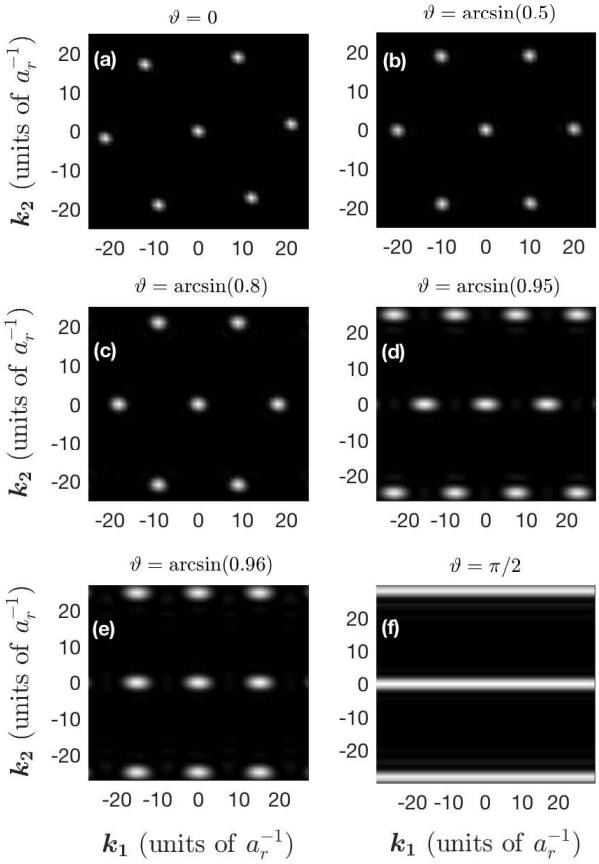

FIG. 7. Static structure factor S. Same parameters as in Fig. 6.

DDI $g_d = g$ and high rotation frequency $\Omega/\omega_r = 0.95$ by imaginary time propagation. As shown in Fig. 6, for polarization predominantly perpendicular to the 2D BEC plane (i.e., $\vartheta \approx 0$), the vortices form a regular triangular lattice [cf. Figs. 6(a)–(c)]. The corresponding structure factor in Figs. 7(a)–(c) reveals a hexagonal reciprocal primitive cell, characteristic of the triangular lattice. As the polarization axis rotates into the plane of the BEC, the vortex lattice aligns with the polarization axis [cf. Figs. 6(d)–(f)]. Parallel polarization (i.e., $\vartheta \approx \pi/2$) is observed in Figs. 6(e)–(f), and the vortex lattice becomes nearly rectangular. In the extreme case with $\vartheta = \pi/2$, the vortices align on a central 1D line that splits the BEC into two fragments. The elongation in each BEC fragment is caused by magnetostriction, which tends to align dipoles in a head-to-tail configuration (for positive DDI). From the Fourier transform $\hat{U}_{\rm dd}^{\rm 2D}$, the DDI between the two fragments is repulsive but drops exponentially in momentum for short wavelength [48, 49]. The distance between the fragments is $\simeq 2.5a_r$, which is on the order of μm. For polarization angles which are slightly less than $\pi/2$, instead of a single split we observe that the whole condensate splits into several fragments [cf. Figs. 6(e)]. The effective contact interaction $\bar{g} = 0$ for $\vartheta = \pi/2$ and $\bar{g} = 3\sqrt{\frac{\gamma}{2\pi}}g(1 - \sin^2\vartheta) \geq 0.29g$ for other ϑ shown in Fig. 6 (a)-(e). For increasing ϑ, the dominant contact interaction strength $\bar{g}$ is decreasing and the number of vortices is decreasing (similar to the conventional BEC system without DDI [1–3]), which shows that larger interactions result in more vortices under the same rotational frequency.

In Fig. 8, we show densities of the rotating dipolar BEC for different polarization angles ϑ and different DDI strength with a very fast rotational frequency $\Omega/\omega_r = 0.99$, which nearly equals to its ultimate limit $\Omega/\omega_r = 1.0$. It is observed that the change of a triangular vortex lattice structure to a rectangular vortex lattice structure occurs when both the polarization angle ϑ and the natural dimensionless parameter $\varepsilon_{dd} := g_d/g$ are close to their limits $\vartheta = \pi/2$ and $\varepsilon_{dd} = 1.0$. For dipoles oriented along the z-axis ($\vartheta = 0$), the 2D system described by Eq. (3) is invariant under the axis rotation, i.e. if $\phi_g(\boldsymbol{\rho})$ is a ground state, $\phi_g(R\boldsymbol{\rho})$ ($R \in SO(2)$) is also a ground state. Moreover, for any polarization angle ϑ, Eq. (3) possesses the symmetry that if $\phi_g(x, y)$ is a ground state, $\overline{\phi}_g(-x, y)$ and $\overline{\phi}_g(x, -y)$ are also ground states. Therefore, for $\vartheta = 0$, the vortex lattice state plotted in Fig. 8 (a) will still be a possible configuration after arbitrary rotation and/or reflection about x axis. For the other dipole orientations partially or fully lying in the xy-plane, the rotational invariant symmetry of the 2D BEC breaks and only the reflection symmetry about the x and the y axes remains, the vortex lattice density plots shown in Fig. 8 with $\vartheta \in (0, \pi/2]$ are the only possible configurations.

For the negative DDI strength, there are more vortices found in the condensate for in-plane polarization of the DDI ($\vartheta = \pi/2$) rather than off-plane polarizations ($\vartheta = 0$), which is in contrast with the positive DDI strength case but agrees well with the behaviour of effective contact interaction $\bar{g}$. This evidence implies that the number of vortices are still mainly

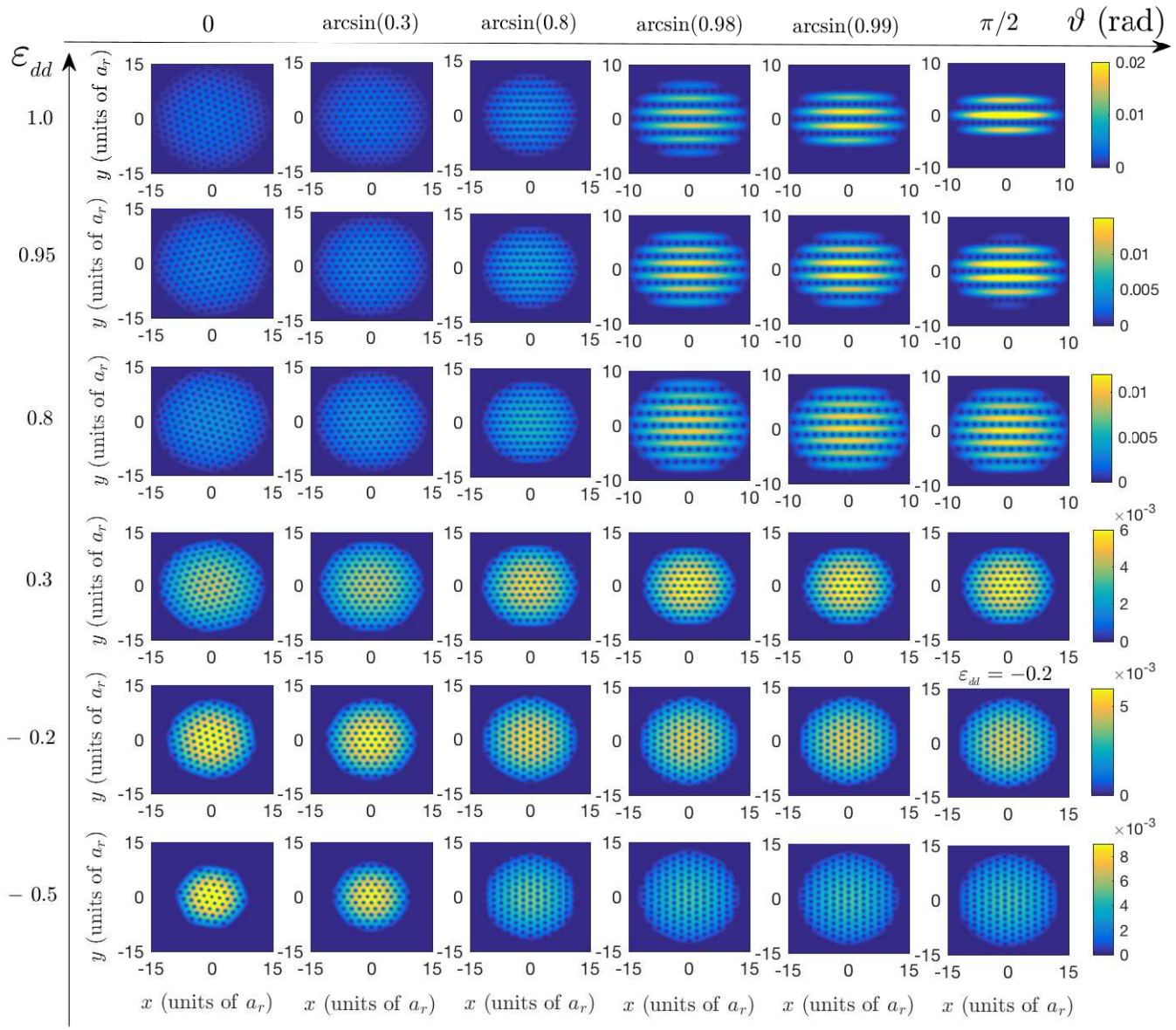

FIG. 8. (Color online) Density of a rotating dipolar BEC for different dipole polarization angles with $\varphi = 0$ and $\vartheta = 0,\ \arcsin(0.3),\ \arcsin(0.8),\ \arcsin(0.98),\ \arcsin(0.99),\ \pi/2$ (from left to right) and for different DDI strengths with $\varepsilon_{dd} = -0.5, -0.2, 0.3, 0.8, 0.95, 1.0$ (from bottom to top). The rotation frequency is $\Omega/\omega_r = 0.99$, $\gamma = 10$ and $g = 250$.

determined by the effective contact interaction $\bar{g}$. On the other hand, the DDI significantly affects the distribution of the vortices (cf. Figs. 7 and 8). As discussed earlier, for such $\vartheta \in (0, \pi/2]$, positive DDI aligns the dipoles along the in-plane polarization x axis, while negative DDI aligns the dipoles along the y axis perpendicular to the polarization x axis, resulting in a very different vortex lattice orientation as shown in Fig. 8. We find that the vortices are arranged in a similar way, i.e., the vortices with negative DDI strengths are aligned perpendicular to the polarization x axis, while the vortices with positive DDI strengths are aligned parallel to the polarization x axis.

In Fig. 9, we show the angle $\eta = \angle(\boldsymbol{k}_1, \boldsymbol{k}_2)$ between the basis vectors $\boldsymbol{k}_1$ and $\boldsymbol{k}_2$ of the reciprocal lattice defined through the structure factor in Eq. (5). For positive DDI strength, as ϑ increases from 0, η starts from $\pi/3$ and varies rather slowly initially; at a critical angle around $\arcsin(0.95)$, η exhibits a jump to the value of $\pi/2$, indicating a structural change to a rectangular vortex lattice. In contrast, for negative DDI strength, η stays near $\pi/3$ as ϑ changes from 0 to $\pi/2$, hence the vortex lattice remains roughly triangular independent of the polarization angle.

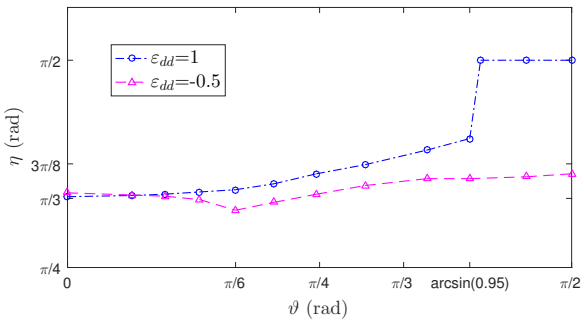

FIG. 9. Lattice orientation parameter η vs ϑ. Same parameters as in Fig. 6.

V. CONCLUSIONS

We have studied the change of the critical rotational frequency versus the s-wave contact interaction strength, the DDI strength and the varying polarization direction $\mathbf{n} = (\sin\vartheta, 0, \cos\vartheta)$. We find that the critical rotational frequency is monotonically decreasing with growing s-wave contact interaction strength g, and identically approaches the confinement frequency limit for $g, g_d \approx 0$. The critical rotation frequency drops rapidly near $g = 0$ and then decreases more and more slowly for large g. In contrast to previous works, our results cover both the case of $g_d > 0$ and $g_d < 0$, and it is observed that the effect of the polarization angle ϑ to the critical rotation frequency depends on the sign of g_d. Specifically, the critical rotational frequency increases (decreases) with varying ϑ from 0 to $\pi/2$ for fixed positive (negative) DDI g_d. In addition, we find numerically that at the 'magic angle' $\vartheta = \arccos(\sqrt{3}/3) \approx 54.7^{\circ}$, the critical rotational frequency is almost independent of the value of DDI strength.

We have numerically simulated the dipolar GPE under fast rotation limit and show different patterns of vortex lattices which strongly depend on the polarization direction. When the polarization angle ϑ changes from perpendicular to parallel to the condensate plane, a structural phase transition in the vortex geometry from triangle to square is observed for positive g_d, but not for negative g_d. This result is consistent with the analytical results of Martin *et al.* [34]. Meanwhile, by plotting the static structure factor and the orientation parameter η of the vortex lattice, we find evidence that the lattice orientation varies with the polarization angle ϑ.

ACKNOWLEDGMENTS

This work was partially supported by the National Natural Science Foundation of China Grants 11771036 and U1530401 (Y.C.), 11601148 (Y.Y.), the Academic Research Fund of Ministry of Education of Singapore grant R-146-000-223-112 (M.R. and W.B.) and the US NSF and the Welch Foundation Grant No. C-1669 (H.P.).

[1] A. J. Leggett, Rev. Mod. Phys. **73**, 307 (2001).
[2] A. L. Fetter, Rev. Mod. Phys. **81**, 647 (2009).
[3] H. Saarikoski, S. M. Reimann, A. Harju, and M. Manninen, Rev. Mod. Phys. **82**, 2785 (2010).
[4] T. Lahaye, C. Menotti, L. Santos, M. Lewenstein, and T. Pfau, Rep. Prog. Phys. **72**, 126401 (2009).
[5] M. A. Baranov, Phys. Rep. **464**, 71 (2008).
[6] K. Góral, K. Rzążewski, and T. Pfau, Phys. Rev. A **61**, 051601 (2000).
[7] S. Yi and L. You, Phys. Rev. A **61**, 041604 (2000).
[8] L. Santos, G. V. Shlyapnikov, P. Zoller, and M. Lewenstein, Phys. Rev. Lett. **85**, 1791 (2000).
[9] L. Santos, G. V. Shlyapnikov, and M. Lewenstein, Phys. Rev. Lett. **90**, 250403 (2003).
[10] U. R. Fischer, Phys. Rev. A **73**, 031602 (2006).
[11] R. M. W. van Bijnen, D. H. J. O'Dell, N. G. Parker, and A. M. Martin, Phys. Rev. Lett. **98**, 150401 (2007).
[12] S. Yi and L. You, Phys. Rev. A **63**, 053607 (2001).
[13] H. P. Büchler, E. Demler, M. Lukin, A. Micheli, N. Prokof'ev, G. Pupillo, and P. Zoller, Phys. Rev. Lett. **98**, 060404 (2007).
[14] K. Góral, L. Santos, and M. Lewenstein, Phys. Rev. Lett. **88**, 170406 (2002).
[15] A. Micheli, G. K. Brennen, and P. Zoller, Nat. Phys. **2**, 341 (2006).
[16] A. Griesmaier, J. Werner, S. Hensler, J. Stuhler, and T. Pfau, Phys. Rev. Lett. **94**, 160401 (2005).
[17] J. Stuhler, A. Griesmaier, T. Koch, M. Fattori, T. Pfau, S. Giovanazzi, P. Pedri, and L. Santos, Phys. Rev. Lett. **95**, 150406 (2005).
[18] T. Koch, T. Lahaye, J. Metz, B. Fröhlich, A. Griesmaier, and T. Pfau, Nat. Phys. **4**, 218 (2008).
[19] K. Aikawa, A. Frisch, M. Mark, S. Baier, A. Rietzler, R. Grimm, and F. Ferlaino, Phys. Rev. Lett. **108**, 210401 (2012).
[20] M. Lu, N. Q. Burdick, S. H. Youn, and B. L. Lev, Phys. Rev. Lett. **107**, 190401 (2011).
[21] M. Fattori, G. Roati, B. Deissler, C. D'Errico, M. Zaccanti, M. Jona-Lasinio, L. Santos, M. Inguscio, and G. Modugno, Phys. Rev. Lett. **101**, 190405 (2008).
[22] M. Vengalattore, S. R. Leslie, J. Guzman, and D. M. Stamper-Kurn, Phys. Rev. Lett. **100**, 170403 (2008).
[23] T. Vogt, M. Viteau, J. Zhao, A. Chotia, D. Comparat, and P. Pillet, Phys. Rev. Lett. **97**, 083003 (2006).
[24] K. K. Ni, S. Ospelkaus, D. Wang, G. Quemener, B. Neyenhuis, M. H. G. de Miranda, J. L. Bohn, J. Ye, and D. S. Jin, Nature **464**, 1324 (2010).
[25] M. H. G. de Miranda, A. Chotia, B. Neyenhuis, D. Wang, G. Quemener, S. Ospelkaus, J. L. Bohn, J. Ye, and D. S. Jin, Nat. Phys. **7**, 502 (2011).
[26] A. C. Voigt, M. Taglieber, L. Costa, T. Aoki, W. Wieser, T. W. Hänsch, and K. Dieckmann, Phys. Rev. Lett. **102**, 020405 (2009).
[27] N. R. Cooper, E. H. Rezayi, and S. H. Simon, Phys. Rev. Lett. **95**, 200402 (2005).
[28] N. R. Cooper, E. H. Rezayi, and S. H. Simon, Solid State Commun. **140**, 046 (2006).
[29] J. Zhang and H. Zhai, Phys. Rev. Lett. **95**, 200403 (2005).
[30] S. Yi and H. Pu, Phys. Rev. A **73**, 061602 (2006).

[31] Y. Zhao, J. An, and C.-D. Gong, Phys. Rev. A **87**, 013605 (2013).

[32] Q. Zhao and Q. Gu, Chin. Phys. B **1**, 016702 (2016).

[33] F. Malet, T. Kristensen, S. M. Reimann, and G. M. Kavoulakis, Phys. Rev. A **83**, 033628 (2011).

[34] A. M. Martin, N. G. Marchant, D. H. J. O'Dell, and N. G. Parker, J. Phys.: Condens. Matter **29**, 103004 (2017).

[35] C. Reichhardt, C. J. Olson, R. T. Scalettar, and G. T. Zimányi, Phys. Rev. B **64**, 144509 (2001).

[36] H. Pu, L. O. Baksmaty, S. Yi, and N. P. Bigelow, Phys. Rev. Lett. **94**, 190401 (2005).

[37] S. Giovanazzi, A. Görlitz, and T. Pfau, Phys. Rev. Lett. **89**, 130401 (2002).

[38] W. Bao and Y. Cai, Kinet. Relat. Models **6**, 135 (2013).

[39] W. Bao, Y. Cai, and H. Wang, J. Comput. Phys. **229**, 7874 (2010).

[40] W. Bao, Q. Tang, and Y. Zhang, Commun. Comput. Phys. **19**, 1141 (2016).

[41] Z. Huang, P. A. Markowich, and C. Sparber, Kinet. Relat. Mod. **3**, 181 (2010).

[42] X. Antoine, Q. Tang, and Y. Zhang, Commun. Comput. Phys. **24**, 966 (2018).

[43] L. Pitaevskii and S. Stringari, *Bose-Einstein Condensation* (Oxford University Press, Oxford, 2003).

[44] We will focus on typical parameters available in the experiments. For ^{52}Cr, the ratio $\varepsilon_{\rm dd} = g_{dd}/g$ between the DDI strength g_{dd} and the contact interaction strength g is $\varepsilon_{\rm dd} = 0.16$ [16, 17], while tuning the contact interaction strength g by Feshbach resonance and possibly modifying DDI g_d by rotating magnetic field, the range of $\varepsilon_{\rm dd} \in [-0.5, 1]$ would be possible, which is sufficient and necessary for the existence of the ground state. For Dy and Er atoms with strong DDI, $\varepsilon_{\rm dd} > 1$ and the system is not stable, higher order Lee-Huang-Yang correction term [50] and/or three body interaction [51, 52] may be included to guarantee the existence of ground state, but it is out of the scope of current study, and we restrict to the pure two body contact interaction case with $\varepsilon_{\rm dd} \in [-0.5, 1]$.

[45] D. S. Petrov, M. Holzmann, and G. V. Shlyapnikov, Phys. Rev. Lett. **84**, 2551 (2000).

[46] Y. Cai, M. Rosenkranz, Z. Lei, and W. Bao, Phys. Rev. A **82**, 043623 (2010).

[47] S. Yi and H. Pu, Phys. Rev. A **73**, 061602 (2006).

[48] M. A. Baranov, A. Micheli, S. Ronen, and P. Zoller, Phys. Rev. A **83**, 043602 (2011).

[49] M. Rosenkranz and W. Bao, Phys. Rev. A **84**, 050701 (2011).

[50] R. N. Bisset, R. M. Wilson, D. Baillie, and P. B. Blakie, Phys. Rev. A **94**, 033619 (2016).

[51] R. N. Bisset and P. B. Blakie, Phys. Rev. A **92**, 061603 (2015).

[52] K.-T. Xi and H. Saito, Phys. Rev. A **93**, 011604 (2016).